ACADEMIC PRESS

Available online at www.sciencedirect.com

SCIENCE DIRECT®

Journal of Magnetic Resonance 159 (2002) 213–218

JMR Journal of Magnetic Resonance

www.academicpress.com

Quantification of B_0 homogeneity variation with head pitch by registered three-dimensional field mapping

J. Michael Tyszka[a,*] and Adam N. Mamelak[b]

[a] *Division of Molecular Medicine, Beckman Research Institute of the City of Hope, Duarte, CA, USA*
[b] *Division of Surgery, City of Hope National Medical Center, Duarte, CA, USA*

Received 8 July 2002; revised 17 October 2002

Abstract

In this study, we quantify the extent to which B_0 homogeneity in adult humans is dependent on head pitch relative to the B_0 vector. Three-dimensional, whole-brain B_0 field maps were acquired in five normal subjects for three generalized head pitch angles. Optimal first- and second-order shimming of the experimental B_0 maps were simulated numerically. The spatial B_0 distribution within the brain was analyzed following automated volumetric co-registration of all data. Increasing head pitch improves both the resonance offset and local homogeneity in the inferior frontal lobes, but introduces inhomogeneities in other regions of the brain which cannot be compensated by first-order shimming but are further improved by second-order shimming.

Keywords: Magnetic resonance imaging; Magnetic resonance spectroscopic imaging; Magnetic field homogeneity; Shimming; Head pitch

1. Introduction

Static magnetic field (B_0) homogeneity is a fundamental concern during the design and implementation of most magnetic resonance experiments. Magnetic resonance spectroscopic imaging (MRSI) [1–5] is particularly vulnerable to macroscopic B_0 inhomogeneities, since water and lipid suppression must be extremely effective over large volumes of tissue. Rapid gradient-echo sequences for echo-planar imaging and T_2^*-weighted functional MRI are similarly sensitive to macroscopic susceptibility gradients, which cause intra-voxel dephasing with associated signal attenuation, and potentially uncorrectable geometric distortions [6,7]. Intrinsic B_0 inhomogeneities due to susceptibility differences between air and tissue are particularly profound in the inferior frontal and temporal lobes of the human brain neighboring the nasal cavity and temporal bones [7].

Current shim coils are the traditional compensation for B_0 inhomogeneities arising from susceptibility differences between tissue, bone, and surrounding air spaces. Most clinical systems generate only first-order Legendre polynomial terms, which allow adequate shimming of small volumes for localized spectroscopy and spectroscopic imaging, and first-order compensation for global residual field gradients. The improvements in B_0 homogeneity following the addition of linear and non-linear polynomial shim terms have been thoroughly quantified by Spielman et al. [4] and strongly support the use of second-order and higher polynomial terms. Other studies suggest that B_0 inhomogeneities in the human brain have significant spatial components up to ninth-order [8], prompting the development of a ferroshimming insert customized to each patient. This latter approach has a relatively complex implementation, typically requiring customized ferroshim designs for each patient and relies on accurate head positioning relative to the shim insert [9].

Earlier studies employing finite element analysis (FEA) and experimental B_0 mapping established the

* Corresponding author. Present address: Beckman Institute 139-74, California Institute of Technology, 1200 E California Blvd, Pasadena, CA 91125, USA. Fax: 1-310-855-0137.
E-mail address: jmt@caltech.edu (J. Michael Tyszka).

1090-7807/02/$ - see front matter © 2002 Elsevier Science (USA). All rights reserved.
PII: S1090-7807(02)00101-5

general character of B_0 inhomogeneities in the adult human brain, but stopped short of exploring the field variation with head pitch angle [10,11]. More recently, improvements in B_0 homogeneity with increased head pitch as suggested by Smith and Collins [12] have been described following both 3D FEA [13] and experimental two-dimensional B_0 mapping [14]. In these studies, an improvement in local homogeneity was observed in the inferior frontal and temporal lobes as the chin was raised away from the chest (increasing head pitch).

In this paper, we extend the experimental work of Heberlein and Hu [14] from two-dimensional single-slice data to full three-dimensional B_0 mapping of the whole head. We also introduce automatic volumetric co-registration of B_0 maps to build a more complete picture of B_0 homogeneity differences between different head pitch angles.

2. Materials and methods

2.1. Data acquisition

All data were acquired using an LX EchoSpeed MRI system (General Electric Medical Systems, Milwaukee, WI) equipped with a 22 mT/m gradient set capable of a maximum slew rate of 120 T/m/s. Complex MR images for B_0 field mapping were acquired with a custom-written volumetric double-echo gradient-echo sequence [15]. Echo times of 4.34 and 8.68 ms were chosen to place water and fat in phase throughout the excited volume, allowing the separation of B_0 and chemical shift. Data were acquired with the following imaging parameters: TR = 12 ms, $32 \times 32 \times 32$ voxels, 26 cm × 26 cm × 26 cm field of view, one signal average, total acquisition time 14 s.

Five control subjects (mean ± SD age = 30.4 ± 9.5 years, 3 males, 2 females) with no history of neurological problems were recruited in accordance with a protocol approved by the Institutional Review Board at our facility.

For this study, we define pitch as rotation about the left-right anatomic axis of the head, with increasing pitch angle equivalent to reducing the angle between the main magnetic field vector and the anterior commissure to posterior commissure (AC–PC) line. Each subject was positioned supine within the quadrature head coil and asked to hold their head at three different pitch angles: neck flexed ("chin down"), head held in a neutral position, and neck extended ("chin up"). Padding was placed beneath the neck or head to help the subject maintain a given pitch angle. No attempt was made to control the exact head pitch angle, since this would be calculated retrospectively from the co-registration transformation.

2.2. Image processing

All data were transferred to a Precision 620 workstation (Dell Computer, Austin, TX) for image processing and analysis. All processing was performed in Matlab (The Mathworks, Natick, MA) using a combination of custom written and proprietary functions, except for regression analysis in Excel (Microsoft, Redmond, WA). The raw, complex gradient-echo images were initially Fourier resampled with radial Hamming filtering to $64 \times 64 \times 64$. B_0 was initially calculated for all voxels.Unwrapping of the B_0 maps was performed using a weighted predictive region growing algorithm adapted from the Synthetic Aperture Radar (SAR) literature [16]. The unwrapping algorithm was designed to be robust to the closely spaced phase discontinuities present in both SAR data and B_0 phase images. Multiple weighted extrapolations from previously unwrapped voxels were used to improve the estimate of the true phase of a neighboring wrapped voxel during region growing. The regions for unwrapping were defined using a mask derived from the mean of the first and second echo magnitude images. The signal intensity of the mean echo image was normalized to the range 0–1 and the mask generated from all voxels with an intensity greater than 0.25. Regions in which the intra-voxel phase dispersion lead to near complete signal loss were excluded by the intensity mask. The mask was finally reapplied to the unwrapped B_0 map to remove low signal regions which remained wrapped. A volume-of-interest (VOI) containing only the brain, and excluding surrounding tissues, was traced manually for each dataset from the magnitude images prior to registration and subsequent processing. This was not prohibitively time-consuming, considering the low resolution of the data, and the small number of subjects.

All B_0 maps were synthetically shimmed by optimized fitting of first- or second-order Legendre shim polynomials to all voxels within the volume defined by the logical AND of the manually defined brain VOI and the magnitude VOI used for B_0 calculation (subsequently called the combined VOI). This served two purposes: first, to eliminate residual systematic errors following automatic linear shimming by the MR system and second, to allow numerical assessment of the effect of second-order shimming which was not available on the MR system used for these experiments. For reference, the first- and second-order Legendre shim polynomials in Cartesian coordinates and their conventional labels are: x ("X"), y ("Y"), z ("Z"), xy ("XY"), xz ("XZ"), yz ("YZ"), $x^2 - y^2$ ("X2 – Y2"), and $z^2 - \frac{1}{2}(x^2 + y^2)$ ("Z2").

All brain VOI masked magnitude data were registered to the neutral pitch image of one subject using a 12-parameter affine transform optimization (rotation, scaling, skew, and translation in three spatial dimensions) implemented by the AIR 5 package (available

from http://bishopw.loni.ucla.edu/AIR5/index.html) [17, 18] running under Cygwin (Red Hat, Durham, NC). The resulting 4×4 transform matrix was then used to resample the magnitude images, combined VOI mask and synthetically shimmed B_0 maps.

The relative pitch change required to co-register the data was recovered from the 3×3 sub-matrix representing the transform without displacement $\mathbf{T} = \mathbf{QS}$, where $\mathbf{Q}$ is the orthogonal rotation matrix and $\mathbf{S}$ is the upper-triangular skew/scaling matrix. $\mathbf{Q}$ and $\mathbf{S}$ can be recovered from $\mathbf{T}$ by Cholesky factorization, chol$(\cdot)$, as follows:

$$\mathbf{T}'\mathbf{T} = (\mathbf{QS})' \cdot (\mathbf{QS}) = \mathbf{S}'\mathbf{Q}'\mathbf{QS} = \mathbf{S}'\mathbf{S} \tag{1}$$

since $\mathbf{Q}$ is orthogonal. $\mathbf{T}'\mathbf{T}$ is positive definite and symmetric providing that the elements of $\mathbf{T}$ are real, so, by definition

$$\mathbf{S} = \text{chol}(\mathbf{T}' \cdot \mathbf{T}) \tag{2}$$

and

$$\mathbf{Q} = \mathbf{TS}^{-1}. \tag{3}$$

The rotation axis and angle are then recovered from the rotation matrix $\mathbf{Q}$ using the following relations [19]:

$$\theta = \cos^{-1}\left(\frac{\text{Tr}(\mathbf{Q}) - 1}{2}\right) \tag{4}$$

and

$$\hat{\mathbf{r}} = \frac{1}{2\sin(\theta)}\begin{pmatrix} Q_{32} - Q_{23} \\ Q_{13} - Q_{31} \\ Q_{21} - Q_{12} \end{pmatrix}, \tag{5}$$

where θ is the rotation angle about $\hat{\mathbf{r}}$, Tr$(\cdot)$ is the trace operator, and Q_{ij} are the matrix elements of $\mathbf{Q}$. The use of a general rotation angle and axis assumes that $\hat{\mathbf{r}}$ is approximately perpendicular to both $\mathbf{B}_0$ and the AC–PC line.

Two measures of B_0 homogeneity were calculated: global B_0 distribution within the combined VOI and local B_0 distribution within a moving $3 \times 3 \times 3$ voxel kernel ($12\,\text{mm} \times 12\,\text{mm} \times 12\,\text{mm}$). Mean local linewidth was calculated from the mean registered B_0 maps for each of the three nominal head pitches. The resonance linewidth for both global and local B_0 measures was estimated from the standard deviation of B_0 within the VOI or kernel assuming a Gaussian distribution using the relation:

$$\Delta f_{\text{FWHM}} = \text{SD}(B_0)\sqrt{8\log 2}. \tag{6}$$

3. Results and discussion

Calculated co-registration head pitch angles show a predictable spread of rotations within each nominal position group. The mean and standard deviation of the measured pitch angle for each group were as follows: chin down, $-30.8° \pm 4.2°$; head neutral, $-12.3° \pm 9.1°$; chin up, $21.8° \pm 4.3°$. Since the subjects' heads were not constrained externally, the neutral and down pitch distributions overlap slightly. The up and down pitch angle groups demonstrated relatively small angular variances compared to the neutral pitch position.

Comparison of the mean, registered B_0 maps for all subjects reveals a pattern of improving local and global homogeneity within the brain as the pitch of the head increases (Figs. 1 and 2). Linear regression of linewidth against head pitch (Fig. 3) gives slopes for first-order shimming of −0.00159 ppm/degree

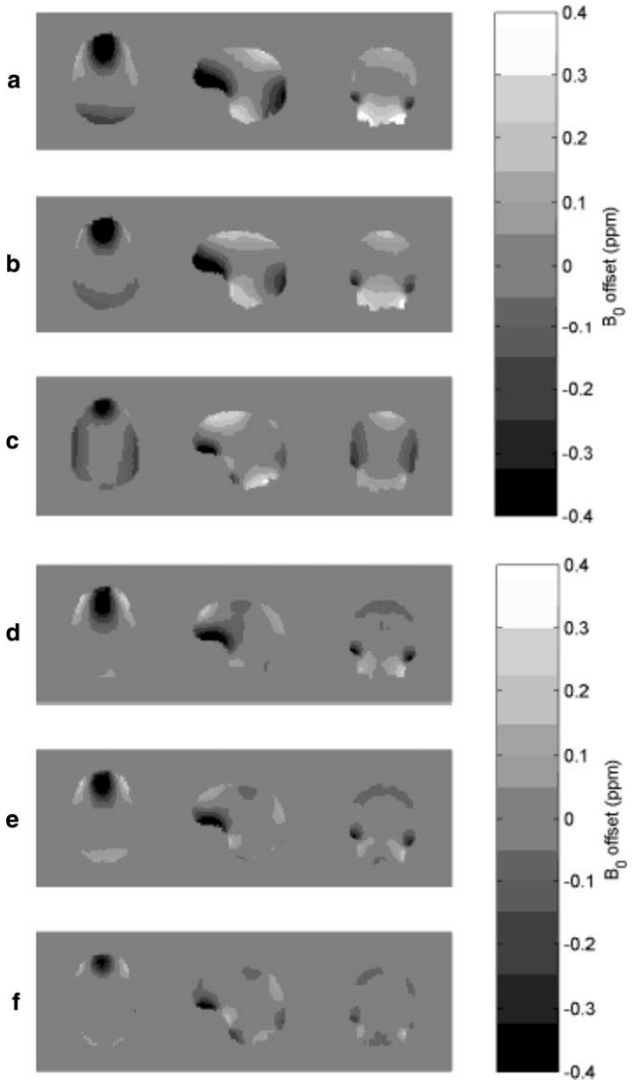

Fig. 1. Mean registered B_0 maps calculated from all five subjects for each head position: chin down (a,d), head neutral (b,e), and chin up (c,f). The maps were calculated following synthetic linear (a–c) and second-order (d–f) shimming prior to registration and averaging. The central axial (left column), sagittal (middle), and coronal (right) sections through the data are shown. The improvement in homogeneity as the head tilts up is most evident in the inferior regions of the frontal and temporal lobes.

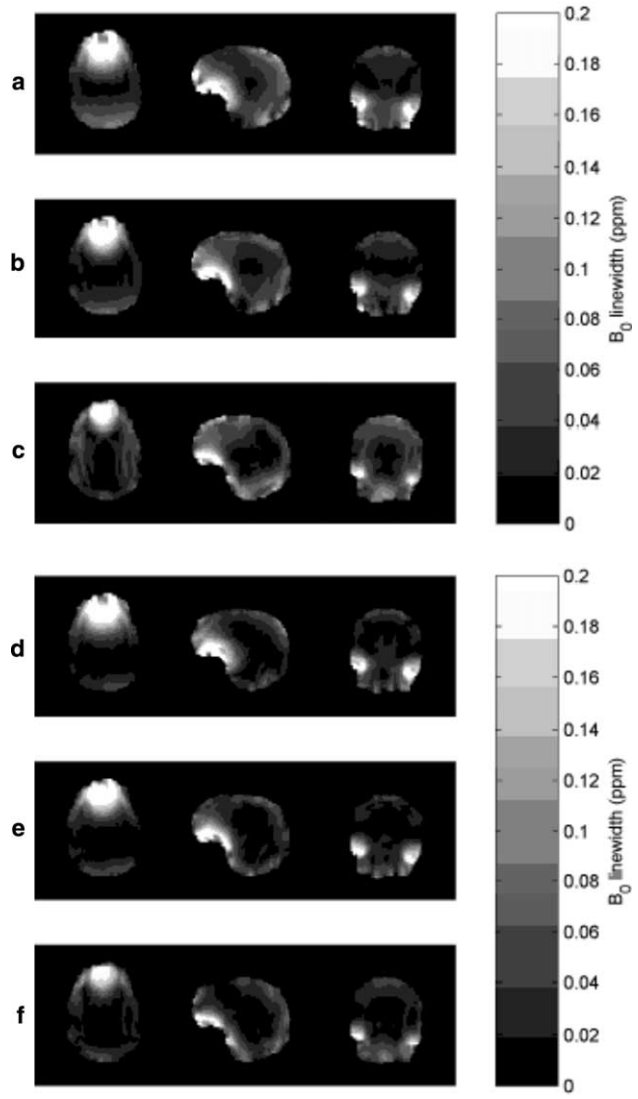

Fig. 2. Local linewidth maps calculated from the mean registered B_0 maps of Fig. 1. The local linewidth was estimated from the standard deviation of the B_0 distribution within a moving $3 \times 3 \times 3$ voxel kernel assuming a Gaussian lineshape. The extent of the regions with increased line-broadening in the inferior frontal and temporal lobes decreases with increasing head pitch and shim order.

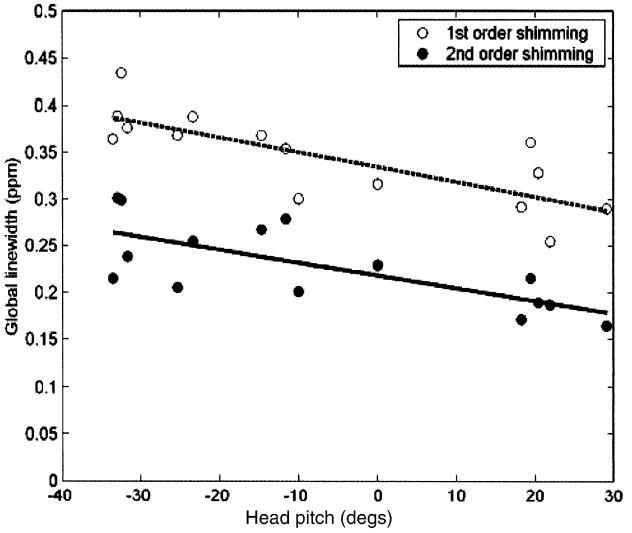

Fig. 3. Variation of global B_0 linewidth with co-registration head pitch angle for all 15 B_0 maps acquired from five subjects. Estimated global linewidths decrease consistently with both increasing head pitch and shimming order. Linear regression results for the first-order shimmed (dotted line) and second-order shimmed (solid line) B_0 maps are shown.

($r = -0.780$, $p = 0.0006$, $n = 15$) and for second-order shimming of $-.00136$ ppm/degree ($r = -0.719$, $p = 0.0025$, $n = 15$).

The empirical cumulative density function (CDF) of the local linewidth distributions for each nominal head pitch and simulated shim order were calculated (Fig. 4). The CDF indicates the total number of voxels within the combined VOI for which B_0 is less than or equal to a given value, normalized to the total number of voxels in the VOI. These CDFs show that following first-order shimming, the nominal "neutral" head position provides more voxels with lower linewidths up to 0.065 ppm, above which the "chin up" position is more favorable. Following second-order shimming, the "chin up" position has consistently better local homogeneity statistics than the other two positions.

Comparison between pooled results from different nominal head pitches was possible following volumetric co-registration (Fig. 5). Only the "neutral" and "chin up" pitches are compared here, since these represent routine positioning and the position most likely to improve homogeneity respectively. Changes in resonance offset were compared by considering the difference between absolute B_0 offsets, $|B_0^{\text{neutral}}| - |B_0^{\text{up}}|$, and the difference in local line-widths, $\Delta f_{\text{FWHM}}^{\text{neutral}} - \Delta f_{\text{FWHM}}^{\text{up}}$. Positive values in each case indicate an improvement in B_0 offset or local homogeneity in the "chin up" position. Following ideal first-order shimming, large regions of the inferior frontal lobes show reduced absolute resonance offsets in excess of 1 ppm in the "chin up" position (Fig. 5a). However, this is countered by increased absolute offsets in the superior frontal and lateral margins of the brain. Second-order shimming appears to be able to compensate for these deficits (Fig. 5b). Improvements in the local linewidth with increased head pitch are similarly most pronounced in the inferior frontal lobes, with ideal second-order shimming (Fig. 5d) reducing a linewidth deficit in the brain stem which is not fully compensated by first-order shimming (Fig. 5c).

These results reflect the changes in relative position of the nasal cavity, temporal bones, and inferior regions of the frontal and temporal lobes as head pitch increases as previously observed by Heberlein and Hu [14] and Truong et al. [13]. Susceptibility artifacts associated with air/tissue or bone/tissue interfaces are

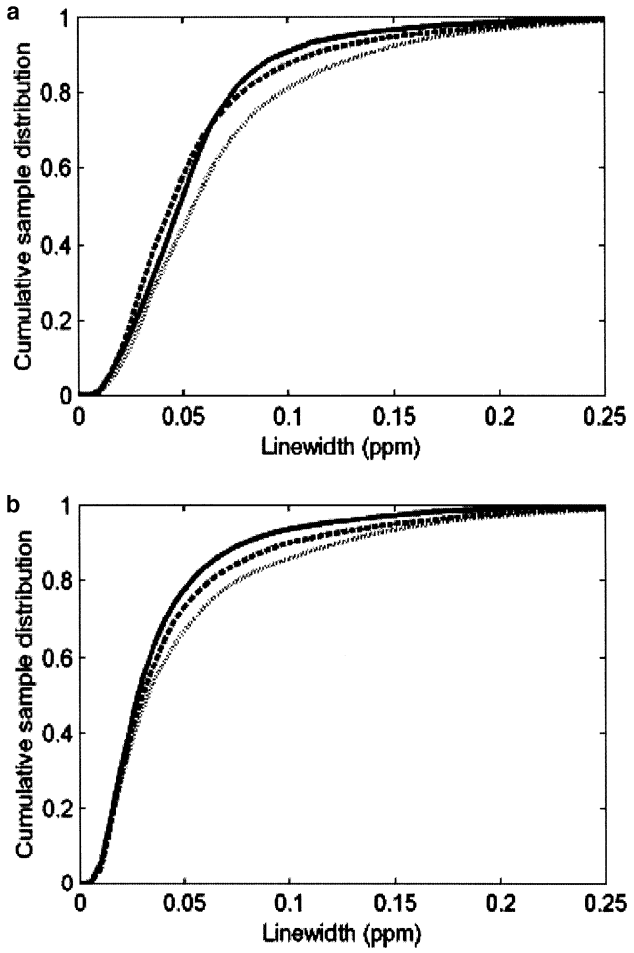

Fig. 4. Cumulative sample distributions for local linewidth calculated from the mean registered B_0 maps within the brain VOI for each of the nominal head pitches: chin down (fine dotted), neutral (dashed), and chin up (solid). Simulated cumulative distributions are shown following: (a) first-order and (b) second-order shimming.

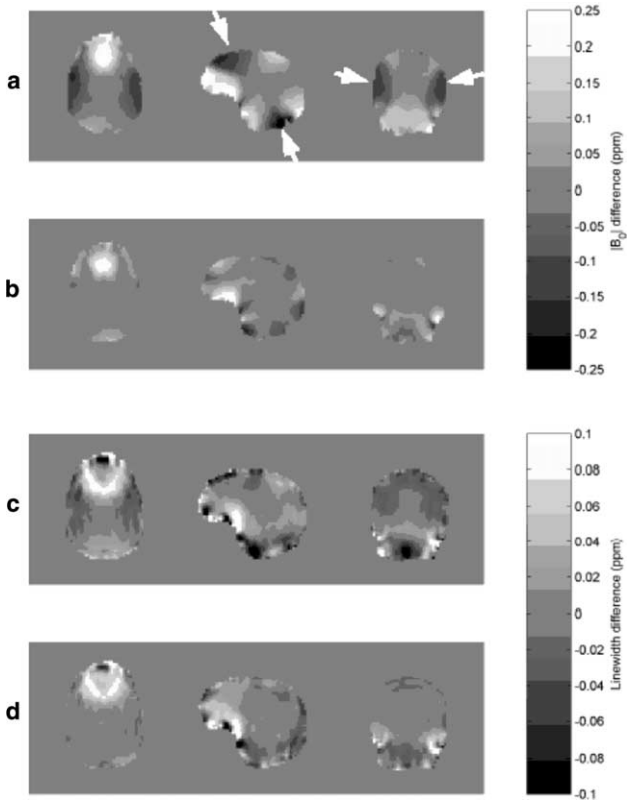

Fig. 5. Pooled absolute B_0 difference $|B_0^{\text{neutral}}| - |B_0^{\text{up}}|$ (a,b) and local B_0 linewidth difference (c,d) between the head neutral position typical of most MRI examinations and the head up position following 3D co-registration of the image volumes. Positive values indicate regions in which the "chin up" position reduces resonance offset or local linewidth and can be considered an improvement in B_0 homogeneity. Note that, following ideal linear shimming, several regions are further from resonance in the "chin up" position compared to the neutral position (arrows).

most pronounced along the B_0 vector direction. As the head pitch increases, the nasal cavity rotates from under the frontal lobes, placing the associated susceptibility artifact more anterior relative to the frontal lobes. A similar effect is seen in the inferior regions of the temporal lobes.

Both of these regions have proven problematic for any B_0 inhomogeneity sensitive acquisition, such as MRSI or fMRI. Since most clinical MRI systems are not equipped with shim orders greater than first order, increasing the head pitch provides a convenient, though incomplete compensation for B_0 inhomogeneities neighboring the skull-base.

The results presented here demonstrate broad trends in the B_0 homogeneity of the brain averaged across a group of normal adults. Specific, highly localized variations should be expected very close to air/tissue interfaces which depend on the unique anatomic geometry of a given subject and cannot be predicted from inter-subject averaged B_0 maps.

4. Conclusion

In general, both global and local measures of B_0 homogeneity improve with increasing head pitch. Improvements are most pronounced in the inferior frontal lobes. However, these local improvements are associated with an increased resonance offset in lateral and superior regions of the frontal and temporal lobes which are not corrected by first-order shimming. Combining second-order shimming with increased head pitch provides more consistent improvements in local and global B_0 homogeneity.

Acknowledgments

This work was supported in part by a grant from the Kogan Foundation. We thank Dr. Keith Heberlein for generously providing copies of cited work.

References

[1] E. Adalsteinsson, P. Irarrazabal, S. Topp, C. Meyer, A. Macovski, D.M. Spielman, Volumetric spectroscopic imaging with spiral-based *k*-space trajectories, Magn. Reson. Med. 39 (1998) 889–898.

[2] E. Adalsteinsson, D.M. Spielman, Spatially resolved two-dimensional spectroscopy, Magn. Reson. Med. 41 (1999) 8–12.

[3] J.M. Tyszka, A.N. Mamelak, Volumetric multishot echo-planar spectroscopic imaging, Magn. Reson. Med. 46 (2001) 219–227.

[4] D.M. Spielman, E. Adalsteinsson, K.O. Lim, Quantitative assessment of improved homogeneity using higher-order shims for spectroscopic imaging of the brain, Magn. Reson. Med. 40 (1998) 376–382.

[5] S.J. Nelson, D.B. Vigneron, J. Star-Lack, J. Kurhanewicz, High spatial resolution and speed in MRSI, NMR Biomed. 10 (1997) 411–422.

[6] K.D. Merboldt, J. Finsterbusch, J. Frahm, Reducing inhomogeneity artifacts in functional MRI of human brain activation—Thin sections vs gradient compensation, J. Magn. Reson. 145 (2000) 184–191.

[7] J.G. Ojemann, E. Akbudak, A.Z. Snyder, R.C. McKinstry, M.E. Raichle, T.E. Conturo, Anatomic localization and quantitative analysis of gradient refocused echo-planar fMRI susceptibility artifacts, Neuroimage 6 (1997) 156–167.

[8] A. Jesmanowicz, P. Starewicz, J.S. Hyde, Determination of shims needed for correction of tissue susceptibility effects in fMRI, in: Proceedings of the Eighth Scientific Meeting of the International Society of Magn. Reson. Med., Denver, CO, 2000, p. 1378.

[9] A. Jesmanowicz, V. Roopchansingh, R.W. Cox, P. Starewicz, W.F.B. Punchard, J. Hyde, Local ferroshims using office copier toner, in: Proceedings of the Ninth Scientific Meeting of the International Society of Magn. Reson. Med., Glasgow, Scotland, 2001, p. 617.

[10] S.Z. Li, B.J. Dardzinski, C.M. Collins, Q.X. Yang, M.B. Smith, Three-dimensional mapping of the static magnetic field inside the human head, Magn. Reson. Med. 36 (1996) 705–714.

[11] S.Z. Li, G.D. Williams, T.A. Frisk, B.W. Arnold, M.B. Smith, A Computer-simulation of the static magnetic-field distribution in the human head, Magn. Reson. Med. 34 (1995) 268–275.

[12] M.B. Smith, C. Collins, Shimming high field magnets, in: Proceedings of the Seventh Annual Meeting of the International Society of Magnetic Resonance in Medicine (Weekend Educational Program), Philadelphia, PA, 1999.

[13] T.-K. Truong, B.D. Clymer, D.W. Chakeres, P. Schmalbrock, Three-dimensional numerical simulations of susceptibility-induced magnetic field inhomogeneities in the human head at 8 T, in: Proceedings of the Tenth Annual Meeting of the International Society of Magnetic Resonance in Medicine, Honolulu, Hawaii, 2002, p. 2323.

[14] K. Heberlein, X. Hu, Improved shim by subject head positioning, in: Proceedings of the Ninth Annual Meeting of the International Society of Magnetic Resonance in Medicine, Glasgow, Scotland, 2001, p. 1157.

[15] H. Wen, F.A. Jaffer, An in vivo automated shimming method taking into account shim current constraints, Magn. Reson. Med. 34 (1995) 898–904.

[16] W. Xu, I. Cumming, A region growing algorithm for InSAR phase unwrapping, in: Proceedings of the IEEE International Geoscience and Remote Sensing Symposium, Lincoln, NE, USA, 1996, pp. 2044–2046.

[17] R.P. Woods, J.C. Mazziotta, S.R. Cherry, MRI-PET registration with automated algorithm, J. Comput. Assist. Tomogr. 17 (1993) 536–546.

[18] R.P. Woods, S.T. Grafton, C.J. Holmes, S.R. Cherry, J.C. Mazziotta, Automated image registration: I. General methods and intrasubject intramodality validation, J. Comput. Assist. Tomogr. 22 (1998) 139–152.

[19] M.E. Pique, Rotation tools, in: A.S. Glassner (Ed.), Graphics Gems, Academic Press, Boston, 1990, pp. 466–467.